Adaptive Finite Element Approximation of Fluid-Structure Interaction Based on an Eulerian Variational Formulation

Thomas Dunne and Rolf Rannacher

Institute of Applied Mathematics, University of Heidelberg, INF 294/293, 69120 Heidelberg, Germany

Abstract. We propose a general variational framework for the adaptive finite element approximation of fluid-structure interaction problems. The modeling is based on an Eulerian description of the (incompressible) fluid as well as the (elastic) structure dynamics. This is achieved by tracking the movement of the initial positions of all 'material' points. In this approach the deformation appears as a primary variable in an Eulerian framework. Our approach uses a technique which is similar to the *Level Set* method in so far that it also tracks initial data, in our case the set of *Initial Positions*, and from this determines to which 'phase' a point belongs. To avoid the need for reinitialization of the initial position set, we employ the harmonic continuation of the structure velocity field into the fluid domain. Based on this monolithic model of the fluid-structure interaction we apply the *dual weighted residual method* for goal-oriented a posteriori error estimation and mesh adaptation to fluid-structure interaction problems. Several stationary as well as nonstationary examples are presented.

1 Introduction

Computational fluid dynamics and computational structure mechanics are two major areas of numerical simulation of physical systems. With the introduction of high performance computing it has become possible to tackle systems with a coupling of fluid and structure dynamics. General examples of such fluid-structure interaction (FSI) problems are flow transporting elastic particles (particulate flow), flow around elastic structures (airplanes, submarines) and flow in elastic structures (haemodynamics, transport of fluids in closed containers). In all these settings the dilemma in modeling the coupled dynamics is that the fluid model is normally based on an Eulerian perspective in contrast to the usual Lagrangian approach for the solid model. This makes the setup of a common variational description difficult. However, such a variational formulation of FSI is needed as the basis of a consistent approach to residual-based a posteriori error estimation and mesh adaptation as well as to the solution of optimal control problems by the Euler-Lagrange method. This is the subject of the present paper.

Combining the Eulerian and the Lagrangian setting for describing FSI involves conceptional difficulties. On the one hand the fluid domain itself is

time-dependent and depends on the deformation of the structure domain. On the other hand, for the structure the fluid boundary values (velocity and the normal stress) are needed. In both cases values from the one problem are used for the other, which is costly and can lead to a drastic loss of accuracy. A common approach to dealing with this problem is to separate the two models, solve each separately, and so converge iteratively to a solution which satisfies both together with the interface conditions (Figure 1). Solving the separated problems serially multiple times is referred to as a 'partitioned approach'.

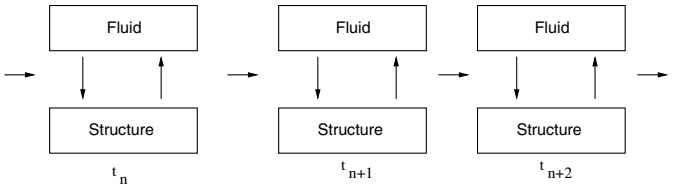

Fig. 1. Partitioned approach, Lagrangian and Eulerian frameworks coupled.

A partitioned approach does not contain a variational equation for the fluid-structure interface. To achieve this, usually an auxiliary unknown coordinate transformation function ζ_f is introduced for the fluid domain. With its help the fluid problem is rewritten as one on the transformed domain which is fixed in time. Then, all computations are done on the fixed reference domain and as part of the computation the auxiliary transformation function ζ_f has to be determined at each time step. Figure 2 illustrates this approach for the driven cavity problem considered in Section 5, below. Such, so-called 'arbitrary Lagrangian-Eulerian' (ALE) methods are used in [17,31,16], and corresponding transformed space-time finite element formulations in [27,28].

Both, the partitioned and the transformation approach to overcome the Euler-Lagrange discrepancy explicitly track the fluid-structure interface by

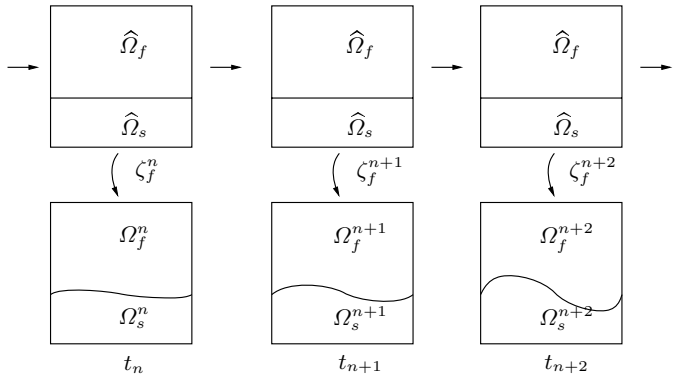

Fig. 2. Transformation approach, both frameworks Lagrangian

mesh adjustment and are generally referred to as 'interface tracking' methods. Both methods leave the structure problem in its natural Lagrangian setting.

In this paper, we follow the alternative way of posing the fluid as well as the structure problem in a fully Eulerian framework. A similar approach has been used by Lui and Walkington [21] in the context of the transport of visco-elastic bodies in a fluid. In the Eulerian setting a phase variable is employed on the fixed mesh to distinguish between the different phases, liquid and solid. This approach to identifying the fluid-structure interface is generally referred to as 'interface capturing', a method commonly used in the simulation of multiphase flows, [18,19]. Examples for the use of such a phase variable are the Volume of Fluid (VoF) method [14] and the Level Set (LS) method [9,22,26]. In the classical LS approach the distance function has to continually be reinitialized, due to the smearing effect by the convection velocity in the fluid domain. This makes the use of the LS method delicate for modeling FSI problems particularly in the presence of cornered structures. To cope with this difficulty, we propose a variant of the LS method that makes reinitialization unnecessary and which easily cope with cornered structures.

The method we describe does not depend on the specific structure model. The key variable in structure dynamics is the deformation, and since this depends on the deflection, it is understandable why structure dynamics is preferably described in the Lagrangian frame. To be able to describe the deformations in the Eulerian frame, we introduce the set of 'initial positions' (IP set) of all structure points. This set is then transported with the structure velocity in each time step. Based on the IP set points and their Eulerian coordinates the displacement is now available in an Eulerian sense. Also its gradient has to be rewritten appropriately, which will be explained later in Section 3.2. Since the fluid-structure interface will be crossing through cells, we will have to also transport the IP set in the fluid domain.

If we were to use the fluid velocity for the convection of the IP set, this would lead to entanglement of the respective displacements, which would 'wreak havoc' on the interface cells. This is a known problem with LS approaches. A common way for fixing this problem has been to occasionally fix the LS field between the time steps. The problem with this approach is that the variational formulation is no longer consistent. As an alternative, we harmonically continue the structure velocity into the fluid domain. In the fluid domain we then use this velocity for the convection of the IP set. Since an IP set set is available in both domains, we can always at each point determine if it belongs to the fluid or solid part of the model.

Again this approach is similar to the LS approach. Actually, it is possible to also develop a model for FSI using the level set approach, [20]. But when developing a complete variational formulation the two key characteristics of the LS approach also become the main cause of concern: reinitialization and the signed distance function. Although the problem of reinitialization here can also be avoided by using an harmonically extended velocity, the trouble concerning corner approximation persists. In contrast to this, by using an

initial position set, we are deforming a virtual mesh of the structure which is extended into the whole domain.

The equations we use are based on the momentum and mass conservation equations for the flow of an incompressible Newtonian fluid and the deformation of a compressible St. Venant-Kirchhoff or likewise incompressible neo-Hookean solid. The spatial discretization is by a second-order finite element method with conforming equal-order (bilinear) trial functions using 'local projection stabilization' as introduced by Becker and Braack [2,3]. The time discretization uses the second-order 'Fractional-Step-θ' scheme originally proposed by Bristeau, Glowinski, and Periaux [7]. This method has the same complexity as the Crank–Nicolson scheme but better stability properties, [23].

Based on the Eulerian variational formulation of the FSI system, we use the 'dual weighted residual' (DWR) method, described in [4,5,1], to derive 'goal-oriented' a posteriori error estimates. The evaluation of these error estimates requires the approximate solution of a linear dual variational problem. The resulting a posteriori error indicators are then used for automatic local mesh adaption. The full application of the DWR method to FSI problems requires a Galerkin discretization in space as well as in time. Due to the use of a difference scheme in time, in this paper we are limited to 'goal-oriented' mesh adaptation in computing steady states or (somewhat heuristically) to quasi-steady states within the time stepping process. The incorporation of automatic time-step control will be the subject of forthcoming work.

The method for computing FSI described in this paper is validated at a stationary model problem that is a lid-driven cavity involving the interaction of an incompressible Stokes fluid with a linearized incompressible neo-Hookean solid. Then, as a more challenging test the self-induced oscillation of a thin elastic bar immersed in an incompressible fluid is treated (FLUSTRUK-A benchmark described in [15]). For this test problem, our method is also compared against a standard 'arbitrary Lagrange Eulerian' (ALE) approach. The possible potential of the fully Eulerian formulation of the FSI problems is indicated by its good behavior for large structure deformations. All computations and visualizations are done using the flow-solver package GASCOIGNE [33] and the graphics package VISUSIMPLE [32]. More details on the software implementation can be found in [10].

The outline of this paper is as follows. Section 2 introduces the basic notation for the Eulerian formulation of the FSI problem which is then described in Section 3. Section 4 presents the discretization in space and time and the derivation of a posteriori error estimates and strategies for mesh adaptation. In Section 5 the proposed method is validated at a stationary test problem 'elastic flow cavity'. Finally, Section 6 contains the results obtained for the nonstationary benchmark problem FLUSTRUK-A (oscillations of a thin elastic bar) for various combinations of material models and flow conditions.

2 Notation

We begin with introducing some notation which will be used throughout the paper. By $\Omega \subset \mathbb{R}^d$ ($d = 2$ or $d = 3$), we denote the domain of definition of the FSI problem. The domain Ω is supposed to be *time independent* but to consist of two possibly time-dependent subdomains, the fluid domain $\Omega_f(t)$ and the structure domain $\Omega_s(t)$. Unless needed, the explicit time dependency will be skipped in this notation. The boundaries of Ω, Ω_f, and Ω_s are denote by $\partial\Omega$, $\partial\Omega_f$, and $\partial\Omega_s$, respectively. The common interface between Ω_f and Ω_s is $\Gamma_i(t)$, or simply Γ_i.

The initial structure domain is denoted by $\widehat{\Omega}_s$. Spaces, domains, coordinates, values (such as pressure, displacement, velocity) and operators associated to $\widehat{\Omega}_s$ (or $\widehat{\Omega}_f$) will likewise be indicated by a 'hat'.

Partial derivatives of a function f with respect to the $i-$th coordinate are denoted by $\partial_i f$, and the total time-derivative by $d_t f$. The divergences of vectors and tensors are written as $\mathrm{div} f = \sum_i \partial_i f_i$ and $(\mathrm{div} F)_i = \sum_j \partial_j F_{ij}$. The gradient of a vector valued function v is the tensor $(\nabla v)_{ij} = \partial_j v_i$.

By $[f]$, we denote the jump of a (possibly discontinuous) function f across an interior boundary, where n is always the unit vector n at points on that boundary.

For a set X, we denote by $L^2(X)$ the Lebesque space of square-integrable functions on X equipped with the usual inner product and norm

$$(f,g)_X := \int_X fg\, dx, \quad \|f\|_X^2 = (f,f)_X,$$

respectively, and correspondingly for vector- and matrix-valued functions. Mostly the domain X will be Ω, in which case we will skip the domain index in products and norms. For Ω_f and Ω_s, we similarly indicate the associated spaces, products, and norms by a corresponding index 'f' or 's'.

Let $L_X := L^2(X)$ and $L_X^0 := L^2(X)/\mathbb{R}$. The functions in L_X (with $X = \Omega$, $X = \Omega_f(t)$, or $X = \Omega_s(t)$) with first-order distributional derivatives in L_X make up the Sobolev space $H^1(X)$. Further, $H_0^1(X) = \{v \in H^1(X) : v_{|\partial X_D} = 0\}$, where ∂X_D is that part of the boundary ∂X at which Dirichlet boundary conditions are imposed. Further, we will use the function spaces $V_X := H^1(X)^d$, $V_X^0 := H_0^1(X)^d$, and for time-dependent functions

$$\begin{aligned} \mathcal{L}_X &:= L^2[0,T;L_X], \quad \mathcal{V}_X := L^2[0,T;V_X] \cap H^1[0,T;V_X^*], \\ \mathcal{L}_X^0 &:= L^2[0,T;L_X^0], \quad \mathcal{V}_X^0 := L^2[0,T;V_X^0] \cap H^1[0,T;V_X^*], \end{aligned}$$

where V_X^* is the dual of V_X^0. Again, the X-index will be skipped in the case of $X = \Omega$, and for $X = \Omega_f$ and $X = \Omega_s$ a corresponding index 'f' or 's' will be used.

3 Formulation

In this section, we introduce the Eulerian formulation of the FSI problem.

3.1 Fluid

For the liquid part, we assume a Newtonian incompressible fluid governed by the usual Navier-Stokes equations, i.e., the equations describing conservation of mass and momentum. The (constant) density and kinematic viscosity of the fluid are ρ_f and ν_f, respectively. The equations are written in an Eulerian framework in the time-dependent domain $\Omega_f(t)$. The physical unknowns are the scalar pressure field $p_f \in \mathcal{L}_f$ and the vector velocity field $v_f \in v_f^D + \mathcal{V}_f$. Here, v_f^D is a suitable extension of the prescribed Dirichlet data on the boundaries (both moving or stationary) of Ω_f, and g_1 is a suitable extension to all of $\partial\Omega_f$ of the Neumann data for $\sigma_f \cdot n$ on the boundaries. We have 'hidden' the fluid-structure interface conditions of steadiness of velocity and normal stress in parts of the boundary conditions v_f^D and g_1. These are addressed in Section 3.3, below. We write the fluid equations in variational form: *Find* $\{v_f, p_f\} \in \{v_f^D + \mathcal{V}_f^0\} \times \mathcal{L}_f$, *such that* $v_f(0) = v_f^0$, *and*

$$\begin{aligned}(\rho_f(\partial_t + v_f \cdot \nabla)v_f, \psi^v)_f + (\sigma_f, \epsilon(\psi^v))_f &= (g_1, \psi^v)_{\partial\Omega_f} + (f_1, \psi^v)_f, \\ (\mathrm{div} v_f, \psi^p)_f &= 0,\end{aligned} \tag{1}$$

for all $\{\psi^v, \psi^p\} \in V_f^0 \times L_f$, *where*

$$\sigma_f := -p_f I + 2\rho_f \nu_f \epsilon(v_f), \quad \epsilon(v) := \tfrac{1}{2}(\nabla v + \nabla v^T).$$

3.2 Structure

In the examples in Sections 5 and 6, below, we consider two different types of materials, an 'incompressible neo-Hookean' (INH) material and a compressible elastic material described by the 'St. Venant-Kirchhoff' (STVK) model. These two models will be described in the next two subsections.

The density of the structure is ρ_s. The material elasticity is usually described by a set of two parameters, the Poisson ration ν_s and the Young modulus E_s, or alternatively, the Lamé coefficients λ_s and μ_s. These parameters satisfy the following relations:

$$\begin{aligned}\nu_s &= \frac{\lambda_s}{2(\lambda_s + \mu_s)}, \quad E_s = \mu_s \frac{3\lambda_s + 2\mu_s}{\lambda_s + \mu_s}, \\ \mu_s &= \frac{E_s}{2(1+\nu_s)}, \quad \lambda_s = \frac{\nu_s E_s}{(1+\nu_s)(1-2\nu_s)},\end{aligned}$$

where $\nu_s = \frac{1}{2}$ for incompressible and $\nu_s < \frac{1}{2}$ for compressible material.

Incompressible Neo-Hookean (INH) material: We consider the case of an incompressible neo-Hookean (INH) elastic medium governed by the equations based on conservation of mass and momentum. Usually these equations are formulated in Lagrangian coordinates in the domain $\hat{\Omega}_s$ with the scalar pressure field $\hat{p}_s \in \hat{\mathcal{L}}_f$ and the vector displacement and velocity fields $\hat{u}_s \in \hat{u}^D + \hat{\mathcal{V}}_s^0$, $\hat{v}_s \in \hat{v}_s^D + \hat{\mathcal{V}}_s^0$. Here, $\hat{u}^D$ and $\hat{v}_s^D$ are suitable extensions of the prescribed Dirichlet data on the boundaries of $\hat{\Omega}_s$, and $\hat{g}_2$ is a suitable extension to all of $\partial\hat{\Omega}_s$ of the Neumann data for $\hat{\sigma}_s \cdot n$ on the boundaries. Again, similarly as for the fluid problem, we have 'hidden' the fluid-structure interface conditions of steadiness of velocity and normal stress in parts of the boundary conditions $\hat{v}_s^D$ and $\hat{g}_2$. These are addressed in Section 3.3, below.

For the sake of simplicity, we assume that the only boundary displacement that take place are on $\hat{\Gamma}_i$, i.e.,

$$\hat{u}^D = \hat{v}_s^D = 0 \ \text{ on } \partial\hat{\Omega}_s \setminus \hat{\Gamma}_i.$$

We write these equations in the following variational form: *Find* $\{\hat{u}_s, \hat{v}_s, \hat{p}_s\} \in \{\hat{u}^D + \hat{\mathcal{V}}_s^0\} \times \{\hat{v}_s^D + \hat{\mathcal{V}}_s^0\} \times \hat{\mathcal{L}}_s$, *such that* $\hat{u}_s(0) = \hat{u}_s^0$, $\hat{v}_s(0) = \hat{v}_s^0$, *and*

$$\begin{aligned} (\rho_s d_t \hat{v}_s, \hat{\psi}^u)_{\hat{s}} + (\hat{\sigma}_s \hat{F}^{-T}, \hat{\epsilon}(\hat{\psi}^u))_{\hat{s}} &= (\hat{g}_2, \hat{\psi}^u)_{\partial\hat{\Omega}_s} + (\hat{f}_2, \hat{\psi}^u)_{\hat{s}}, \\ (d_t \hat{u}_s - \hat{v}_s, \hat{\psi}^v)_{\hat{s}} &= 0, \\ (\det\hat{F}, \hat{\psi}^p)_{\hat{s}} &= (1, \hat{\psi}^p)_{\hat{s}}, \end{aligned} \tag{2}$$

for all $\{\hat{\psi}^u, \hat{\psi}^v, \hat{\psi}^p\} \in \hat{V}_s^0 \times \hat{V}_s^0 \times \hat{L}_s$, *where*

$$\hat{F} := I + \hat{\nabla}\hat{u}_s, \quad \hat{\sigma}_s := -\hat{p}_s I + \mu_s(\hat{F}\hat{F}^T - I), \quad \hat{\epsilon}(\hat{\psi}^u) := \tfrac{1}{2}(\hat{\nabla}\hat{\psi}^u + \hat{\nabla}\hat{\psi}^{uT}).$$

St. Venant-Kirchhoff (STVK) material: We consider a compressible elastic material described by the St. Venant-Kirchhoff (STVK) model. As in the case of the incompressible neo-Hookean material, this model is governed by the equations for conservation of mass and momentum. Again these equations are written in Lagrangian form using the same notation as above. *Find* $\{\hat{u}_s, \hat{v}_s\} \in \{\hat{u}^D + \hat{\mathcal{V}}_s^0\} \times \{\hat{v}_s^D + \hat{\mathcal{V}}_s^0\}$, *such that* $\hat{u}_s(0) = \hat{u}_s^0$, $\hat{v}_s(0) = \hat{v}_s^0$, *and*

$$\begin{aligned} (\rho_s d_t \hat{v}_s, \hat{\psi}^u)_{\hat{s}} + (\hat{J}\,\hat{\sigma}_s\,\hat{F}^{-T}, \hat{\epsilon}(\hat{\psi}^u))_{\hat{s}} &= (\hat{g}_2, \hat{\psi}^u)_{\partial\hat{\Omega}_s} + (\hat{f}_2, \hat{\psi}^u)_{\hat{s}}, \\ (d_t \hat{u}_s - \hat{v}_s, \hat{\psi}^v)_{\hat{s}} &= 0, \end{aligned} \tag{3}$$

for all $\{\hat{\psi}^u, \hat{\psi}^v\} \in \hat{V}_s^0 \times \hat{V}_s^0$, *where*

$$\hat{F} := I + \hat{\nabla}\hat{u}_s, \quad \hat{J} := \det\hat{F}, \quad \hat{E} := \tfrac{1}{2}(\hat{F}^T\hat{F} - I),$$

$$\hat{\epsilon}(\hat{\psi}^u) := \tfrac{1}{2}(\hat{\nabla}\hat{\psi}^u + \hat{\nabla}\hat{\psi}^{uT}), \quad \hat{\sigma}_s := \hat{J}^{-1}\hat{F}(\lambda_s(\mathrm{tr}\hat{E})I + 2\mu_s\hat{E})\hat{F}^T.$$

Conversion to Eulerian frame (the IP set approach): To rewrite the above conservation equations in an Eulerian frame, we need the pressure $\hat{p}_s$, displacement $\hat{u}_s$, and its gradient $\hat{\nabla}\hat{u}_s$ expressed in the Eulerian sense, which are denoted by p_s, u_s, and ∇u_s, respectively. There holds $p_s(x) = \hat{p}_s(\hat{x})$ and $u_s(x) = \hat{u}_s(\hat{x})$, or more precisely,

$$p_s(x) = \hat{p}_s(D(x)) = \hat{p}_s(\hat{x}), \quad u_s(x) = \hat{u}_s(D(x)) = \hat{u}_s(\hat{x}), \tag{4}$$

where $D(x)$ is the (inverse) displacement function of points in the deformed domain Ω_s back to points in the initial domain $\hat{\Omega}_s$. The corresponding displacement function is $\hat{D}(\hat{x})$,

$$\begin{aligned} \hat{D} &: \hat{\Omega}_s \to \Omega_s, \quad \hat{D}(\hat{x}) = \hat{x} + \hat{u}_s = x, \\ D &: \Omega_s \to \hat{\Omega}_s, \quad D(x) = x - u_s = \hat{x}. \end{aligned} \tag{5}$$

Since $\det\hat{\nabla}\hat{D} = \det\hat{F} \neq 0$ the displacements D and $\hat{D}$ are well defined.

The immediate difficulty with the relations (4) is that u_s is only implicitly determined by $\hat{u}_s$, since $D(x)$ also depends on u_s. This is unpractical, and we therefore need a direct way of determining the displacement $u(x)$ of a 'material' point located at x with respect to its initial position at point $\hat{x}$. To achieve this, we introduce the so-called *'set of initial positions'* (IP set) $\phi(\Omega)$ of all points of Ω at time t. If we look at a given 'material' point at the position $x \in \Omega$ and the time $t \in (0, T]$, then the value $\phi(t, x)$ will tell us what the initial position of this point was at time $t = 0$. These points are transported in the full domain with a certain velocity w. The convection velocity in the structure will be the structure velocity itself, $w_{|\Omega_s} = v_s$. If the fluid velocity were to be used for convection in the fluid domain, then the displacements there would eventually become very entangled. For this reason we use an alternative velocity. We explain this in more detail in Subsection 3.3, below. With this notation, the mapping ϕ is determined by the following variational problem: *Find* $\phi \in \phi_0 + \mathcal{V}^0$*, such that*

$$(\partial_t\phi + w \cdot \nabla\phi, \psi) = 0 \quad \forall\psi \in V^0. \tag{6}$$

where ϕ_0 is a suitable extension of the Dirichlet data along the boundaries,

$$\begin{aligned} \phi(0, x) &= x, \quad x \in \Omega, \\ \phi(t, x) &= x, \quad \{t, x\} \in (0, T] \times \partial\Omega. \end{aligned}$$

This means that $\hat{x} + \hat{u}(t, \hat{x}) = x$, for any point with the initial position $\hat{x}$ and the position x later at time t. Since $\hat{x} = \phi(0, \hat{x}) = \phi(t, x)$ and $\hat{u}(t, \hat{x}) = u(t, x)$ it follows that

$$x = \phi + u. \tag{7}$$

Using this in the IP set equation (6) yields

$$(\partial_t u - w + w \cdot \nabla u, \psi) = 0 \quad \forall\psi \in V^0.$$

To access the Eulerian deformation, we use an identity of the displacement functions from (5) $D(\hat{D}(\hat{x})) = \hat{x}$. Differentiating this yields

$$(I - \nabla u)(I + \hat{\nabla}\hat{u}) = I \quad \Leftrightarrow \quad \hat{\nabla}\hat{u} = (I - \nabla u)^{-1} - I.$$

Thus, the Cauchy stress tensor σ_s can be written for INH and STVK materials in an Eulerian framework as follows:

$$\sigma_s = \begin{cases} -p_s I + \mu_s(FF^T - I) & \text{(INH material)}, \\ J^{-1}F(\lambda_s(\mathrm{tr}E)I + 2\mu_s E)F^T & \text{(STVK material)}, \end{cases}$$
$$F = I + \hat{\nabla}\hat{u} = (I - \nabla u)^{-1}, \quad J = \det F, \quad E = \tfrac{1}{2}(F^T F - I).$$

Finally, we write the structure equations in the Eulerian framework for both types of materials, INH and STVK.

INH material in Eulerian formulation: We write the structure equations in Eulerian form in the time-dependent domain $\Omega_s(t)$ with the corresponding scalar pressure field p_s and the vector displacement and velocity fields u_s and v_s, respectively. Here, the incompressibility condition $\det(F) = 1$ is replaced by the divergence condition for the velocity. *Find* $\{u_s, v_s, p_s\} \in \{u^D + \mathcal{V}_s^0\} \times \{v_s^D + \mathcal{V}_s^0\} \times \mathcal{L}_s$, *such that* $u_s(0) = u_s^0$, $v_s(0) = v_s^0$, *and*

$$\begin{aligned} (\rho_s(\partial_t v_s + v_s \cdot \nabla v_s), \psi^u)_s + (\sigma_s, \epsilon(\psi^u))_s &= (g_2, \psi^v)_{\partial\Omega_s} + (f_2, \psi^u)_s, \\ (\partial_t u_s - v_s + v_s \cdot \nabla u_s, \psi^v)_s &= 0, \\ (\mathrm{div} v_s, \psi^p)_s &= 0, \end{aligned} \tag{8}$$

for all $\{\psi^u, \psi^v, \psi^p\} \in V_s^0 \times V_s^0 \times L_s$, *where*

$$\sigma_s := -p_s I + \mu_s(FF^T - I), \quad F := (I - \nabla u)^{-1}, \quad \epsilon(\psi^u) = \tfrac{1}{2}(\nabla\psi^u + \nabla\psi^{uT}).$$

STVK material in Eulerian formulation: We write the structure equations in Eulerian form in the time-dependent domain $\Omega_s(t)$ with the corresponding displacement and velocity fields u_s and v_s, respectively. *Find* $\{u_s, v_s\} \in \{u^D + \mathcal{V}_s^0\} \times \{v_s^D + \mathcal{V}_s^0\}$, *such that* $u_s(0) = u_s^0$, $v_s(0) = v_s^0$, *and*

$$\begin{aligned} (\rho_s(\partial_t v_s + v_s \cdot \nabla v_s), \psi^u)_s + (\sigma_s, \epsilon(\psi^u))_s &= (g_2, \psi^u)_{\partial\Omega_s} + (f_2, \psi^u)_s, \\ (\partial_t u_s - v_s + v_s \cdot \nabla u_s, \psi^v)_s &= 0, \end{aligned} \tag{9}$$

for all $\{\psi^u, \psi^v\} \in V_s^0 \times V_s^0$, *where*

$$\begin{aligned} \sigma_s &:= J^{-1}F(\lambda_s(\mathrm{tr}E)I + 2\mu_s E)F^T, \\ F &:= (I - \nabla u)^{-1}, \quad J := \det F, \quad E := \tfrac{1}{2}(F^T F - I). \end{aligned}$$

3.3 The FSI Problem in Eulerian Formulation

Since now both the fluid and the structure equations (1), (8), and (9) for conservation of mass and momentum are written in an Eulerian frame, they can be combined into one unified formulation. Here, the steadiness of velocity across the fluid-structure interface Γ_i is strongly enforced by requiring one common continuous field for the velocity on Ω. The Dirichlet boundary data v_f^D and v_s^D on parts of $\partial\Omega$ are merged into a suitable velocity field $v^D \in V$. Finally, the force balance condition $\sigma_f \cdot n = \sigma_s \cdot n$ on Γ_i now appears as a boundary integral of the jump $[\sigma \cdot n]$ on the right hand side,

$$([\sigma \cdot n], \psi^v)_{\Gamma_i} = \int_{\Gamma_i} (\sigma_f - \sigma_s) \cdot n_f \psi^v \, do.$$

By omitting this boundary integral the (weak) continuity of $\sigma \cdot n$ becomes an implicit condition of the combined variational formulation. The remaining parts of the Neumann data g_1 and g_2 now form the Neumann boundary data on $\partial\Omega$ and are combined to g_3. We write the Cauchy stress tensor for the whole domain as follows:

$$\sigma := \chi_f \sigma_f + \chi_s \sigma_s.$$

Here, χ_f and χ_s are the characteristic functions of Ω_f and Ω_s, respectively, which are determined by the values of the IP-set function ϕ:

$$\chi_f(t,x) = \begin{cases} 1, & \phi(t,x) \in \hat{\Omega}_f \setminus \hat{\Gamma}_i, \\ 0, & \phi(t,x) \in \hat{\Omega}_s, \end{cases} \qquad \chi_s = 1 - \chi_f. \tag{10}$$

The interface Γ_i will usually intersect mesh cells. Due to this, we need a reasonable continuation of the displacement and its gradient from the structure domain into the fluid domain. The value of u in the fluid domain will be determined by the choice of the convection velocity w. If we were to use the fluid velocity this would eventually lead to increasing entanglement, which would necessitate a continual reinitialization of the IP set. As an alternative, we use the harmonic continuation of the structure velocity to the whole domain Ω, which is likewise denoted by w and satisfies

$$(\chi_s(w - v), \psi) + (\chi_f \alpha_w \nabla w, \nabla \psi) = 0, \quad \forall \psi \in V^0, \tag{11}$$

where α_w is a small positive parameter. By this construction, the deflection u_f in the fluid domain becomes an artificial quantity without any real physical meaning, i.e., $d_t u_s = v_s$, but generally $d_t u_f \neq v_f$.

Now, we can combine the formulations (1), (8), (9), (11), and (10) with (7), to obtain a complete variational formulation of the FSI problem in Eulerian formulation. In the case of STVK material the (non-physical) pressure p_s in the structure subdomain is determined as harmonic extension of the flow pressure p_f.

Eulerian formulation of the FSI problem: *Find fields* $\{v, w, u, p\} \in \{v^D + \mathcal{V}^0\} \times \mathcal{V}^0 \times \mathcal{V}^0 \times \mathcal{L}$, *such that* $v(0) = v^0$, $u(0) = u^0$, *and*

$$\begin{aligned}
(\rho(\partial_t v + v \cdot \nabla v), \psi) + (\sigma, \psi) &= (g_3, \psi)_{\partial\Omega} + (f_3, \psi) \quad \forall \psi \in V^0, \\
(\mathrm{div} v, \chi) &= 0 \quad \forall \chi \in L \quad \text{(INH material)}, \\
(\chi_f \mathrm{div} v, \chi) + (\chi_s \alpha_p \nabla p, \nabla \chi) &= 0 \quad \forall \chi \in L \quad \text{(STVK material)}, \\
(\partial_t u - w + w \cdot \nabla u, \psi) &= 0 \quad \forall \psi \in V^0, \\
(\chi_s (w - v), \psi) + (\chi_f \alpha_w \nabla w, \nabla \psi) &= 0 \quad \forall \psi \in V^0,
\end{aligned} \tag{12}$$

where α_p is a small positive constant, $\rho := \chi_f \rho_f + \chi_s \rho_s$ and $\sigma := \chi_f \sigma_f + \chi_s \sigma_s$, with

$$\chi_f := \begin{cases} 1, & x - u \in \hat{\Omega}_f \setminus \hat{\Gamma}_i, \\ 0, & x - u \in \hat{\Omega}_s, \end{cases} \qquad \chi_s = 1 - \chi_f,$$

and

$$\begin{aligned}
\sigma_f &:= -pI + 2\rho_f \nu_f \epsilon(v), \\
\sigma_s &:= \begin{cases} -pI + \mu_s (F F^T - I) & \text{(INH material)}, \\ J^{-1} F (\lambda_s (\mathrm{tr} E) I + 2\mu_s E) F^T & \text{(STVK material)}, \end{cases} \\
F &:= (I - \nabla u)^{-1}, \quad J := \det F, \quad E := \tfrac{1}{2}(F^T F - I).
\end{aligned}$$

In this variational formulation the position of the fluid structure interface Γ_i is implicitly given by the displacement u and the characteristic function χ_s,

$$\Gamma_i(t) = \{x \in \Omega,\ x - u(x,t) \in \hat{\Gamma}_i\}. \tag{13}$$

Notice that the system (12) is *nonlinear* even if the two subproblems are linear, e.g., for a Stokes fluid interacting with a linear elastic structure.

In some situations the solution of an FSI problem may tend to a 'steady state' as $t \to \infty$. For later purposes, we derive the set of equations determining such a steady state solution $\{v^*, w^*, u^*, p^*\} \in \{v^D + V^0\} \times V^0 \times V^0 \times L$. The corresponding limits of the characteristic functions and subdomains are denoted by χ_f^*, χ_s^* and Ω_f^*, Ω_s^*, respectively. Further, the fluid velocity becomes constant in time, $v_f^* := \lim_{t\to\infty} v_{|\Omega_f}$, and the structure velocity vanishes, $v_s^* \equiv 0$, which in turn implies $w^* \equiv 0$. The steady state structure displacement u_s^* is likewise well defined, but the corresponding ('non-physical') fluid displacement is merely defined by $u_f^* = u_f^{\lim} := \lim_{t\to\infty} u_{|\Omega_f}$ and therefore depends on the chosen construction of $w_{|\Omega_f}$ as harmonic extension of $w_{|\Omega_s}$. Actually, it could be defined by any suitable continuation of u_s^* to all of Ω, e.g., by harmonic continuation. On the other hand the steady state pressure p^* is to be determined from the limiting equations. Then, with suitable extensions u^D and v^D of the prescribed Dirichlet data on $\partial\Omega$, the FSI system (12) reduces to the following 'stationary' form (dropping for simplicity the stars):

Eulerian formulation of the 'stationary' FSI problem: *Find* $\{u, v, p\} \in \{u^D + V^0\} \times \{v^D + V^0\} \times L$ *, such that*

$$\begin{aligned} (\rho v \cdot \nabla v, \psi) + (\sigma, \epsilon(\psi)) &= 0 \quad \forall \psi \in V^0, \\ (\mathrm{div} v, \chi) &= 0 \quad \forall \chi \in L \quad \text{(INH material)}, \\ (\chi_f \mathrm{div} v, \chi) + (\chi_s \alpha_p \nabla p, \nabla \chi) &= 0 \quad \forall \chi \in L \quad \text{(STVK material)}, \\ (\chi_f (u - u_f^{\lim}), \psi) + (\chi_s v, \psi) &= 0 \quad \forall \psi \in V^0, \end{aligned} \tag{14}$$

where $\rho := \chi_f \rho_f + \chi_s \rho_s$ and $\sigma := \chi_f \sigma_f + \chi_s \sigma_s$, with

$$\chi_f := \begin{cases} 1, & x - u \in \hat{\Omega}_f \setminus \hat{\Gamma}_i, \\ 0, & x - u \in \hat{\Omega}_s, \end{cases} \qquad \chi_s = 1 - \chi_f,$$

and

$$\begin{aligned} \sigma_f &:= -pI + 2\rho_f \nu_f \epsilon(v), \\ \sigma_s &:= \begin{cases} -pI + \mu_s (FF^T - I) & \text{(INH material)}, \\ J^{-1} F (\lambda_s (\mathrm{tr} E) I + 2\mu_s E) F^T & \text{(STVK material)}, \end{cases} \\ F &:= (I - \nabla u)^{-1}, \quad J := \det F, \quad E := \tfrac{1}{2}(F^T F - I). \end{aligned}$$

4 Discretization

In this section, we detail the discretization in space and time of the FSI problem based on its Eulerian variational formulation (12).

4.1 Mesh Notation

The spatial discretization is by a conforming finite element Galerkin method on meshes $\mathbb{T}_h$ consisting of cells denoted by K, which are (convex) quadrilaterals in 2d or hexaedrals in 3d. The mesh parameter h is a scalar cell-wise constant function defined by $h_{|K} := h_K = \mathrm{diam}(K)$. 'Refinement' of cells is always by bisection, i.e., by joining opposite midpoints of sides or faces. 'Coarsening' of a cell is possible if it has been generated by prior refinement of some 'parent cell'. The 'finest level' of cells of a mesh $\mathbb{T}_h$ consists of all cells that can be removed by coarsening in one sweep. The resulting coarsened mesh is referred to as $\mathbb{T}_{2h}$. To facilitate mesh refinement and coarsening, we allow the cells to have a certain number of nodes that are at the midpoint of sides or faces of neighboring cells. These 'hanging nodes' do not carry degrees of freedom and the corresponding function values are determined by linear or bilinear interpolation of neighboring 'regular' nodal points. For more details on this approach see [8] or [1].

4.2 Galerkin Formulation

For arguments $U = \{v, w, u, p\}$ and $\Psi = \{\psi^v, \psi^w, \psi^u, \psi^p\} \in \mathcal{W} := \mathcal{V} \times \mathcal{V} \times \mathcal{V} \times \mathcal{V}$, we introduce the space-time semilinear form

$$\begin{aligned} A(U)(\Psi) \;:=\; \int_0^T \Big\{ & (\rho(\partial_t v + v \cdot \nabla v), \psi^v) + (\sigma(U), \epsilon(\psi^v)) \\ & + \begin{cases} (\mathrm{div} v, \psi^p) & \text{(INH material)} \\ (\chi_f \mathrm{div} v, \psi^p) + (\chi_s \alpha_p \nabla p, \nabla \psi^p) & \text{(STVK material)} \end{cases} \\ & - (g_3, \psi^v)_{\partial\Omega} - (f_3, \psi^v) + (\partial_t u - w + w \cdot \nabla u, \psi^u) \\ & + (\chi_s (w - v), \psi^w) + (\chi_f \alpha_w \nabla w, \nabla \psi^w) \Big\}\, dt. \end{aligned}$$

With this notation, we can write the variational problem (12) in compact form: *Find* $U \in U^D + \mathcal{W}^0$ *, such that*

$$A(U)(\Psi) = 0 \quad \forall \Psi \in \mathcal{W}^0, \tag{15}$$

where U^D *is an appropriate extension of the Dirichlet boundary and initial data and the space* $\mathcal{W}^0$ *is defined by*

$$\mathcal{W}^0 := \{\Psi \in \mathcal{V}^0 \times \mathcal{V}^0 \times \mathcal{V}^0 \times \mathcal{V}^0,\ \psi^u(0) = \psi^v(0) = 0\}.$$

For discretizing this problem in space, we use equal-order Q_1 finite elements (d-linear shape functions) for all unknowns, where the corresponding finite element spaces are denoted by $L_h \subset L$, $V_h \subset V$, $W_h \subset W$, etc.. Within the present abstract setting the discretization in time is likewise thought as by a Galerkin method, such as the dG(r) ('discontinuous' Galerkin) or the cG(r) ('continuous' Galerkin) method. Here, the dG(0) method is closely related to the backward Euler scheme and the dG(1) method to the Crank–Nicolson scheme. However, in the test computations described below, we have used a Galerkin method only in space but finite difference schemes in time. The full space-time Galerkin framework is mainly introduced as basis for a systematic approach to residual-based a posteriori error estimation as described below.

The spatial discretization by 'equal-order' finite elements for velocity and pressure needs stabilization in order to compensate for the missing 'inf-sup stability'. We use the so-called *'local projection stabilization'* (LPS) introduced by Becker and Braack [2,3]. An analogous approach is also employed for stabilizing the convection in the flow model as well as in the transport equation for the displacement u. We define the mesh-dependent bilinear form

$$(\varphi, \psi)_\delta := \sum_{K \in \mathbb{T}_h} \delta_K \, (\varphi, \psi)_K,$$

$$\delta_K := \alpha \big(\chi_f \rho_f \nu_f h_K^{-2} + \chi_s \mu_s h_K^{-2} + \beta \rho |v_h|_{\infty;K} h_K^{-1} + \gamma |w_h|_{\infty;K} h_K^{-1} \big)^{-1}.$$

Further, we introduce the 'fluctuation operator' $\pi_h : V_h \to V_{2h}$ on the finest mesh level $\mathbb{T}_h$ by $\pi_h = I - P_{2h}$, where $P_{2h} : V_h \to V_{2h}$ is the L^2-projection. The operator π_h measures the fluctuation of a function in V_h with respect to its projection into the next coarser space V_{2h}. With this notation, we define the stabilization form

$$S_\delta(U_h)(\Psi_h) := \int_0^T \Big\{ (\nabla \pi_h p_h, \nabla \pi_h \psi_h^p)_\delta + (\rho v_h \cdot \nabla \pi_h v_h, v_h \cdot \nabla \pi_h \psi_h^v)_\delta + (w_h \cdot \nabla \pi_h u_h, w_h \cdot \nabla \pi_h \psi_h^u)_\delta \Big\}\, dt,$$

where the first term stabilizes the fluid pressure, the second one the INH structure pressure, the third one the transport in the flow model, and the fourth one the transport of the displacement u_h. Then, the stabilized Galerkin approximation of problem (15) reads: *Find* $U_h \in U_h^D + \mathcal{W}_h^0$, *such that*

$$A_\delta(U_h)(\Psi_h) := A(U_h, \Psi_h) + S_\delta(U_h)(\Psi_h) = 0, \quad \forall \Psi_h \in \mathcal{W}_h^0. \tag{16}$$

The LPS has the important property that it acts only on the diagonal terms of the coupled system and that it does not contain any second-order derivatives. However, it is only 'weakly' consistent, as it does not vanish for the continuous solution, but it tends to zero with the right order as $h \to 0$. The choice of the numbers α, β, γ in the stabilization parameter δ_K is, based on practical experience, in our computations $\alpha = 1/2$, and $\beta = \gamma = 1/6$.

4.3 Time Discretization

The discretization in time is by the so-called *'fractional-step-θ scheme'* in which each time step $t_{n-1} \to t_n$ is splitted into three substeps $t_{n-1} \to t_{n-1+\theta} \to t_{n-\theta} \to t_n$. For brevity, we formulate this time stepping method for an abstract differential-algebraic equation (DAE)

$$\begin{bmatrix} M & 0 \\ 0 & 0 \end{bmatrix} \begin{bmatrix} \dot v(t) \\ \dot p(t) \end{bmatrix} + \begin{bmatrix} A(v(t)) & B \\ -B^T & C \end{bmatrix} \begin{bmatrix} v(t) \\ p(t) \end{bmatrix} = \begin{bmatrix} b(t) \\ c(t) \end{bmatrix}, \tag{17}$$

which resembles the operator form of the spatially discretized incompressible Navier-Stokes equations with pressure stabilization. With the parameters $\theta = 1-\sqrt{2}/2 = 0.292893...$, $\theta' = 1-2\theta$, $\alpha \in (1/2, 1]$, and $\beta = 1-\alpha$, the fractional-step-θ scheme reads:

$$\begin{bmatrix} M+\alpha\theta k A^{n-1+\theta} & \theta k B \\ -B^T & C \end{bmatrix} \begin{bmatrix} v^{n-1+\theta} \\ p^{n-1+\theta} \end{bmatrix} = \begin{bmatrix} [M-\beta\theta k A^{n-1}]v^{n-1} + \theta k b^{n-1} \\ c^{n-1+\theta} \end{bmatrix}$$

$$\begin{bmatrix} M+\beta\theta' k A^{n-\theta} & \theta' k B \\ -B^T & C \end{bmatrix} \begin{bmatrix} v^{n-\theta} \\ p^{n-\theta} \end{bmatrix} = \begin{bmatrix} [M-\alpha\theta' k A^{n-1+\theta}]v^{n-1+\theta} + \theta' k b^{n-\theta} \\ c^{n-\theta} \end{bmatrix}$$

$$\begin{bmatrix} M+\alpha\theta k A^{n} & \theta k B \\ -B^T & C \end{bmatrix} \begin{bmatrix} v^{n} \\ p^{n} \end{bmatrix} = \begin{bmatrix} [M-\beta\theta k A^{n-\theta}]v^{n-\theta} + \theta k b_h^{n-\theta} \\ c^{n} \end{bmatrix},$$

where $A^{n-1+\theta} := A(x^{n-1+\theta})$, $b^{n-1} := b(t_{n-1})$, etc.. This scheme is of second order and has a similar work complexity as the well-known Crank–Nicolson scheme (case $\alpha = 1/2$). The fractional-step-θ scheme was originally proposed in form of an operator splitting scheme separating the two complications 'nonlinearity' and 'incompressibility' within each cycle $t_{n-1} \to t_{n-1+\theta} \to t_{n-\theta} \to t_n$. However, it has also very attractive features as a pure time-stepping method. Being *strongly* A-stable, for any choice of $\alpha \in (1/2, 1]$, it possesses the full smoothing property in the case of rough initial data, in contrast to the Crank–Nicolson scheme which is only conditionally smoothing (for $k \sim h^2$). Furthermore, it is less dissipative than most of the other second-order implicit schemes and therefore suitable for computing oscillatory solutions; for more details, we refer to [23], [24], and [11].

For computing steady state solutions, we use a pseudo-time stepping techniques based on the simple (first-order) backward Euler scheme, which in the notation from before reads

$$\begin{bmatrix} M+kA^n & kB \\ -B^T & C \end{bmatrix} \begin{bmatrix} v^n \\ p^n \end{bmatrix} = \begin{bmatrix} Mv^{n-1} + kb_h^{n-1} \\ c^n \end{bmatrix},$$

4.4 Solution of the Algebraic Systems

After time and space discretization, in each substep of the fractional-step-θ scheme (or any other fully implicit time-stepping scheme) a quasi-stationary nonlinear algebraic system has to be solved. This is done by a standard Newton-type method with adaptive step-length selection, in which the transport terms are correctly linearized. Only the stabilization terms and the terms involving the characteristic function χ_f, determining the position of the interface, are treated by a simple functional iteration. In all cases the iteration starts from the values at the preceding time level. The resulting linear subproblems are then solved by the GMRES method with preconditioning by a geometric multigrid method with block-ILU smoothing. Since such an approach is rather standard nowadays, we omit its details and refer to the relevant literature, e.g., [29], [23], or [16].

4.5 Mesh Adaptation

Now, we come to the main issues of this paper, namely the automatic mesh adaptation within the finite element solution of the FSI problem. The computations shown in Sections 5 and 6, below, have been done on three different types of meshes:

- globally refined meshes obtained using several steps of uniform (edge) bisection of a coarse initial mesh,
- locally refined meshes obtained using a purely geometry-based criterion by marking all cells for refinement which have certain prescribed distances from the fluid-structure interface,

– locally refined meshes obtained using a systematic residual-based criteria by marking all cells for refinement which have error indicators above a certain threshold.

The main goal of this project is to employ the *'dual weighted residual method'* (DWR method) for the adaptive solution of FSI problems. This method has been developed in [4] (see also [5] and [1]) as an extension of the duality technique for a posteriori error estimation described in [12]. The DWR method provides a general framework for the derivation of 'goal-oriented' a posteriori error estimates together with criteria of mesh adaptation for the Galerkin discretization of general linear and nonlinear variational problems, including optimization problems. It is based on a complete *variational* formulation of the problem, such as (15) for the FSI problem. In fact, this was one of the driving factors for deriving the Eulerian formulation underlying (15). In order to incorporate also the time discretization into this framework, we have to use a fully space-time Galerkin method, i.e., a standard finite element method in space combined with the dG(r) od cG(r) ('discontinuous' Galerkin or 'continuous' Galerkin) method in time. The following discussion assumes such a space-time Galerkin discretization, though in our test computations, we have used the fractional-step-θ scheme which is a difference scheme. Accordingly, in this paper the DWR method is used only in its stationary form in computing either steady states or intermediate quasi-steady states within the time stepping process.

We begin with the description of the DWR method for the special case of an FSI problem governed by an abstract variational equation such as (15). For notational simplicity, we think the nonhomogeneous boundary and initial data U^D to be incorporated into a linear forcing term $F(\cdot)$, or to be exactly representable in the approximating space $\mathcal{W}_h$. Then, the problem reads as follows: *Find* $U \in U^D + \mathcal{W}^0$*, such that*

$$A(U)(\Psi) = F(\Psi) \quad \forall \Psi \in \mathcal{W}^0. \tag{18}$$

The corresponding (stabilized) Galerkin approximation reads: *Find* $U_h \in U_h^D + \mathcal{W}_h$*, such that*

$$A(U_h)(\Psi_h) + S_\delta(U_h)(\Psi_h) = F(\Psi) \quad \forall \Psi_h \in \mathcal{W}_h^0. \tag{19}$$

Suppose now that the goal of the computation is the evaluation of the value $J(U)$ for some functional $J(\cdot)$ which is defined on $\mathcal{W}$ and (for notational simplicity only) assumed as linear. We want to control the quality of the discretization in terms of the error $J(U - U_h)$. To this end, we introduce the directional derivative

$$A'(U)(\Phi, \Psi) := \lim_{\epsilon \to 0} \frac{1}{\epsilon} \big\{ A(U + \epsilon\Phi)(\Psi) - A(U)(\Psi) \big\}, \quad \Phi, \Psi \in \mathcal{W}^0,$$

the existence of which is assumed.

Remark 1. The above assumption of differentiability may cause concerns in treating the FSI problem since the dependence of the characteristic function $\chi_f(u)$ in (12) on the deflection u is generically not differentiable (only Lipschitzian). However, this non-differentiability is confined to the interface between fluid and structure which can be assumed to form a lower dimensional manifold. Hence, for practical applications, after discretization along the interface, the directional derivative can safely be replaced by a mesh-size dependent difference quotient. This pragmatic approach has proven very successful in similar situation, e.g., for Hencky elasto-plasticity [25].

With the above notation, we introduce the bilinear form

$$L(U,U_h)(\Phi,\Psi) := \int_0^1 A'(U_h + s(U-U_h))(\Phi,\Psi)\,ds,$$

and formulate the 'dual problem'

$$L(U,U_h)(\Phi,Z) = J(\Phi) \quad \forall \Phi \in \mathcal{W}^0. \tag{20}$$

In the present abstract setting the existence of a solution $Z \in \mathcal{W}^0$ of the dual probelm (20) has to be assumed. Now, taking $\Phi = U - U_h \in \mathcal{W}^0$ in (20) and using the Galerkin orthogonality property

$$A(U)(\Psi_h) - A(U_h)(\Psi_h) = S_\delta(U_h)(\Psi_h), \quad \Psi \in \mathcal{W}_h^0,$$

yields the error representation

$$\begin{aligned} J(U-U_h) &= L(U,U_h)(U-U_h,Z) \\ &= \int_0^1 A'(U_h + s(U-U_h))(U-U_h,Z)\,ds \\ &= A(U)(Z) - A(U_h)(Z) \\ &= F(Z-\Psi_h) - A(U_h)(Z-\Psi_h) - S_\delta(U_h)(\Psi_h) \\ &=: \rho(U_h)(Z-\Psi_h) - S_\delta(U_h)(\Psi_h), \end{aligned}$$

where $\Psi_h \in \mathcal{W}^0$ is an arbitrary element, usually taken as the generic nodal interpolant $I_h Z \in \mathcal{W}_h^0$ of Z. For the evaluation of the terms on the right-hand side, we split the integrals in the residual term $\rho(U_h)(Z-\Psi_h)$ into their contribution from the single mesh cells $K \in \mathbb{T}_h$ and integrate by parts. This results in an estimate of the error $|J(U-U_h)|$ in terms of computable local residual terms $\rho_K(U_h)$ multiplied by certain weight factors $\omega_K(Z)$ which depend on the dual solution Z,

$$|J(U-U_h)| \le \sum_{K\in\mathbb{T}_h} \rho_K(U_h)\,\omega_K(Z) + |S_\delta(U_h)(\Psi_h)|. \tag{21}$$

The explicit form of the terms in the sum on the right-hand side will be stated for a special situation below. The second term due to the regularization is usually neglected.

Since the dual solution Z is unknown, the evaluation of the weights $\omega_K(Z)$ requires further approximation. We linearize by assuming

$$L(U, U_h)(\Phi, \Psi) \approx L(U_h, U_h)(\Phi, \Psi) = A'(U_h)(\Phi, \Psi)$$

and use the approximate 'discrete' dual solution $Z_h \in \mathcal{W}_h^0$ defined by

$$A'(U_h)(\Phi, Z_h) = J(\Phi_h) \quad \forall \Phi_h \in \mathcal{W}_h^0. \tag{22}$$

From Z_h, we generate improved approximations to Z in a post-processing step by patchwise higher-order interpolation. For example in 2d, on 2×2-patches of cells in $\mathbb{T}_h$ the 9 nodal values of the piecewise bilinear Z_h are used to construct a patchwise biquadratic function $\tilde{Z}$. This is then used to obtain the approximate error estimate

$$|J(U - U_h)| \approx \eta := \sum_{K \in \mathbb{T}_h} \rho_K(U_h)\, \omega_K(\tilde{Z}) \tag{23}$$

which is the basis of automatic mesh adaptation, [6,1].

Mesh adaptation algorithm. The approach we use for the adaptive refinement of the spatial mesh is straightforward. Particularly, for the refinement criteria there exist much more sophisticated versions, which are not used in this paper for sake of simplicity. Let an error tolerance TOL be give. Then, on the basis of the (approximate) a posteriori error estimate (23), the mesh adaptation proceeds as follows:

1. Compute the primal solution U_h from (19) on the current mesh, starting from some initial state, e.g., that with zero deformation.
2. Compute the solution $\tilde{Z}_h$ of the approximate discrete dual problem (22).
3. Evaluate the cell-error indicators $\eta_K := \rho_K(U_h)\, \omega_K(\tilde{Z}_h)$.
4. If $\eta < TOL$ then accept U_h and evaluate $J(U_h)$, otherwise proceed to the next step.
5. Determine the 30% cells with largest and the 10% cells with smallest values of η_K. The cells of the first group are refined and those of the second group coarsened. Then, continue with Step 1. (Coarsening usually means canceling of an earlier refinement. Further refinement may be necessary to prevent the occurrence of too many hanging nodes. In two dimensions this strategy leads to about a doubling of the number of cells in each refinement cycle. By a similar strategy it can be achieved that the number of cells stays about constant during the adaptation process within a time stepping procedure.)

Remark 2. The error representation (21) has been derived assuming the error functional $J(\cdot)$ as linear. In many applications nonlinear, most often quadratic, error functionals occur. Examples are the spatial L^2-norm error

$J(U_h) := \|(U - U_h)(T)\|^2$ at the end time T of a nonstationary computation or the least-squares cost-functional $\|U_h - \bar{U}\|^2$ of a stationary optimal control problem. For nonlinear (differentiable) error functionals the DWR approach can be extended to yield an error representation of the form (21); see [5,1].

Remark 3. The DWR method can also be applied to optimization problems of the form

$$\min_{q \in Q} J(u,q)\,! \qquad a(u,q)(\psi) = f(\psi)\ \forall \psi \in V,$$

for instance in the context of an FSI setting. To this end we introduce the Lagrangian functional $\mathcal{L}(u,q,\lambda) := J(u,q) + f(\lambda) - a(u,q)(\lambda)$, with the adjoint variable $\lambda \in V$. Its stationary points $\{u,q,\lambda\}$ are possible solutions of the optimization problem. These are determined by the nonlinear variational equation (so-called KKT system)

$$\mathcal{L}'(u,q,\lambda)(\phi,\chi,\psi) = 0 \quad \forall \{\phi,\chi,\psi\} \in V \times Q \times V,$$

which has saddle-point character. For the solutions $\{u_h, q_h, \lambda_h\}$ of the corresponding finite element Galerkin approximation, there are residual-based error estimates available similar to (23); see [5,1].

A stationary special case. We will develop the explicit form of the error representation (21) and the approximate dual problem (22) for the *stationary* FSI model with an 'incompressible neo-Hookean' (INH) solid. We assume the system as being driven only by Dirichlet boundary conditions, i.e., volume and surface forces are zero, $f_3 \equiv 0$ and $g_3 \equiv 0$. Let $\{v,w,u,p\} \in \{v^D + V^0\} \times V^0 \times V^0 \times L$ be a steady state solution of the corresponding FSI model (12) determined by the system (14). In order to simplify the formulation of the corresponding dual problem, we omit higher order terms, e.g., in the Cauchy stress tensor for the structure. Since there is no movement in the structure domain, the mass conservation condition $\mathrm{div} v_s = 0$ is not practical for the sensitivity analysis. For this reason the conservation condition in the structure domain will be $\det(I - \nabla u) = 1$, from which we again omit the higher order terms by approximating $\det(I - \nabla u) - 1 \approx \mathrm{div} u = 0$. Then, the variational formulation of the stationary FSI problem further reduces to

$$A(U)(\Psi) = F(\Psi) \quad \forall \Psi \in W^0, \tag{24}$$

with the (time-independent) semilinear form

$$\begin{aligned} A(U)(\Psi) \ &:= (\rho v \cdot \nabla v, \psi^v) + (\sigma(U), \epsilon(\Psi)) + (\chi_f \mathrm{div} v + \chi_s \mathrm{div} u, \psi^p) \\ &\quad + (\chi_f u + \chi_s v, \psi^u), \end{aligned}$$

and the linear functional $F(\Psi) := (\chi_f u_f, \psi^u)$. Here, the stress-strain relation is given by

$$\sigma(U) = \begin{cases} -pI + 2\rho_f \nu_f \epsilon(v), & \text{in } \Omega_f, \\ -pI + 2\mu_s \epsilon(u), & \text{in } \Omega_s. \end{cases}$$

where the (small-strain) approximation $FF^T - I \approx 2\epsilon(\psi^u)$ has been used.

Suppose now that the discretization error is to be controlled with respect to some linear functional on W of the form $J(\Phi) = \{j^u(\phi^u), j^v(\phi^v), j^p(\phi^p)\}$. In order to correctly set up the corresponding dual problem, we would have to differentiate the semi-linear form $A(U)(\Psi)$ with respect to all components of U. However, this is not directly possible since the unknown position of the interface Γ_i depends on the displacement function u in a non-differentiable way. Because of this difficulty, we will adopt a more heuristic approach which is rather common in solving problems with free, i.e., only implicitly determined, boundaries. We assume that the interface obtained on the current mesh is already in good agreement with the correct one, $\Gamma_{ih} \approx \Gamma_i$, and set up the dual problem formally with Γ_{ih} as a fixed interface.

Adopting these simplifications and dropping all stabilization terms leads us to the following approximate dual problem: *Find* $Z = \{z^u, z^v, z^p\} \in W^0$, *such that*

$$\tilde{A}'(U_h)(\Phi, Z) = J(\Phi) \quad \forall \Phi \in W^0. \tag{25}$$

for all $\Phi = \{\phi^u, \phi^v, \phi^p\} \in W^0$, *with the bilinear form*

$$\begin{aligned} \tilde{A}'(U_h)(\Phi, Z) = {} & (\rho v_h \cdot \nabla \phi^v, z^v) + (\rho \phi^v \cdot \nabla v_h, z^v) + (\sigma'(U_h)\epsilon(\Phi), \epsilon(Z)) \\ & + (\chi_f \mathrm{div} \phi^v + \chi_s \mathrm{div} \phi^u, z^p) + (\chi_f \phi^u + \chi_s \phi^v, z^u), \end{aligned}$$

where

$$\sigma'(U_h)\epsilon(U) := \begin{cases} -pI + 2\rho_f \nu_f \epsilon(v), & \text{in } \Omega_{f,h}, \\ -pI + 2\mu_s \epsilon(u), & \text{in } \Omega_{s,h}. \end{cases}$$

Remark 4. The solvability of the dual problem (25) is not for granted and has to be established by exploiting the particular properties of the primal problem (24). This is a difficult task in view of the rather few existence results in the literature for general FSI problems. However, in our test calculation, we have never encountered difficulties in obtaining the 'discrete' dual solution. In the test example considered in Section 5, below, the discrete dual problem has been set up simply by transposing the Newton matrix at the final solution.

Let Z be a solution of (25) and Z_h its finite element approximation. To evaluate the approximate error estimate

$$J(E) \approx F(Z - Z_h) - A(U_h)(Z - Z_h),$$

for $E := U - U_h$, we introduce two modified submeshes

$$\mathbb{T}_{hs} := \{K \cap \Omega_{s,h},\, K \in \mathbb{T}_h\}, \quad \mathbb{T}_{hf} := \{K \cap \Omega_{f,h},\, K \in \mathbb{T}_h\},$$

and their union $\tilde{\mathbb{T}}_h := \mathbb{T}_{hs} \cup \mathbb{T}_{hf}$. The mesh $\tilde{\mathbb{T}}_h$ differs only from $\mathbb{T}_h$ in so far that the cells that contain the fluid-structure interface are subdivided into fluid domain part and structure domain part. Now, by cellwise integration by parts and rearranging boundary terms, we obtain

$$J(E) = \sum_{K\in\tilde{\mathbb{T}}_h} \Big\{ (\mathrm{div}\sigma(U_h) - \rho v_h \cdot \nabla v_h, z^v - z_h^v)_K - (\tfrac{1}{2}[\sigma(U_h)\cdot n], z^v - z_h^v)_{\partial K} \\ - (\chi_f \mathrm{div} v_h + \chi_s \mathrm{div} u_h, z^p - z_h^p)_K - (\chi_f(u_h - u_f) + \chi_s v_h, z^u - z_h^u)_K \Big\},$$

where $[\cdot]$ denotes the jump across intercell boundaries Γ. If Γ is part of the boundary $\partial\Omega$ the 'jump' is assigned the value $[\sigma\cdot n] = 2\sigma\cdot n$. We note that in this error representation the 'cell residuals' $\{\mathrm{div}\sigma(U_h) - \rho v_h\cdot\nabla v_h\}_{|K}$, $\{\chi_f \mathrm{div} v_h + \chi_s \mathrm{div} u_h\}_{|K}$, and $\{\chi_f(u_h - u_f) + \chi_s v_h\}_{|K}$ represent the degree of consistency of the approximate solution U_h, while the 'edge term' $\frac{1}{2}[\sigma(U_h)\cdot n]$ measures its 'discrete' smoothness. These residual terms are multiplied by the weights (sensitivity factors) $z^v - z_h^v$, $z^p - z_h^p$, and $z^u - z_h^u$, respectively. From this error representation, we can deduce the following error estimate

$$|J(E)| \approx \sum_{K\in\tilde{\mathbb{T}}_h} \eta_K, \quad \eta_K := \sum_{i=1}^{4} \rho_K^{(i)} \omega_K^{(i)}, \tag{26}$$

with the residual terms and weights

$$\begin{aligned}
\rho_K^{(1)} &:= \|\mathrm{div}\sigma(U_h) - \rho v_h\cdot\nabla v_h\|_K, \quad \omega_K^{(1)} := \|Z - Z_h\|_K, \\
\rho_K^{(2)} &:= \tfrac{1}{2} h_K^{-1/2} \|[\sigma(U_h)\cdot n]\|_{\partial K}, \quad \omega_K^{(2)} := h_K^{1/2} \|z^v - z_h^v\|_{\partial K}, \\
\rho_K^{(3)} &:= \|\chi_f \mathrm{div} v_h + \chi_s \mathrm{div} u_h\|_K, \quad \omega_K^{(3)} := \|z^p - z_h^p\|_K, \\
\rho_K^{(4)} &:= \|\chi_f(u_h - u_f) + \chi_s v_h\|_K, \quad \omega_K^{(4)} := \|z^u - z_h^u\|_K.
\end{aligned}$$

The weights $\omega^{(i)}$ are approximated, for instance by post-processing the discrete dual solution Z_h. Then, the cellwise error indicators η_K can be used for the mesh adaptation process as described above.

5 Numerical Test 1: Elastic Flow Cavity

For validating the numerical method described in the preceding section, we use a simple stationary test example, the lid-driven cavity with an elastic bottom wall, as shown in Figure 3. For simplicity, for modeling the fluid the linear Stokes equations are used and the material of the bottom wall is assumed to be linear neo-Hookean and incompressible. The structure material is taken as very soft such that a visible deformation of the fluid-structure interface can be expected. Then, the other material parameters are chosen such that flow and solid deformation velocity are small enough to allow for a

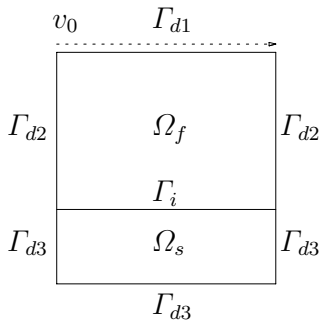

Fig. 3. Configuration of the 'elastic' lid-driven cavity.

stationary solution of the coupled linear systems. This solution is computed by a pseudo-time stepping method employing the implicit Euler scheme. A steady state is reached once the kinetic energy of the structure is below a prescribed small tolerance, here $\|v_s\|^2 \leq 10^{-8}$.

The cavity has a size of 2×2, and its elastic part has a height of 0.5. The material constants are $\rho_f = \rho_s = 1$, $\nu_f = 0.2$, and $\mu_s = 2.0$. At the top boundary Γ_{d1} the regularized tangential flow profile

$$v_0 = 0.5 \begin{cases} 4x, & x \in [0.0, 0.25], \\ 1, & x \in (0.25, 1.75), \\ 4(2-x), & x \in [1.75, 2.0], \end{cases}$$

is prescribed, in order to avoid problems due to pressure singularities.

5.1 Computations on Globally Refined Meshes

Figure 6 shows the development of $\|v_s\|^2$ during the pseudo-time stepping process depending on the number of cells of the mesh. As expected the kinetic energy tends to zero. The multiple 'bumps' occur due to the way the elastic structure reaches its stationary state by 'swinging' back and forth a few times. At the extreme point of each swing the kinetic energy has a local minimum. Figures 4 and 5 show the final stationary state computed on globally uniform meshes. In Figure 7, we monitor the mass error of the structure at the stationary state and find that it is actually of the expected order $O(h^2)$.

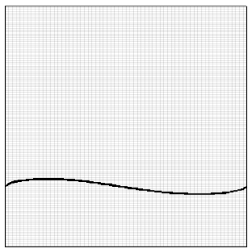

Fig. 4. Final position of interface.

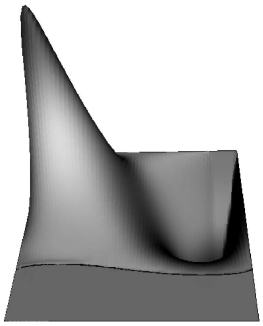

Fig. 5. Vertical velocity.

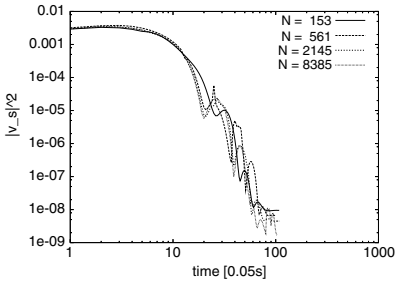

Fig. 6. Variation of $\|v_s\|^2$ in time for different numbers N of mesh cells.

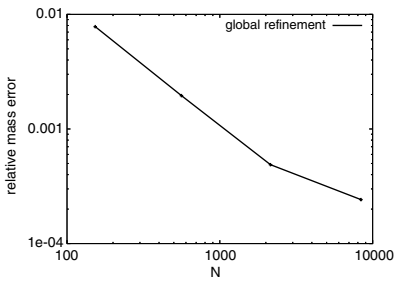

Fig. 7. Relative error of mass conservation in the steady state on globally and locally refined meshes.

5.2 Computations on Locally Adapted Meshes

Next, we apply the simplified stationary version of the DWR method as described in Subsection 4.5 for local mesh adaptation in the present test problem. For the 'goal-oriented' a posteriori error estimation, we take the value of the pressure at the point $A = (0.5, 1.0)^T$ which is located in the flow region. To avoid sharp singularities in the corresponding dual solution, the associated functional is regularized to

$$J(u,p) = |K_A|^{-1} \int_{K_A} p\,dx \approx p(A),$$

where $K_A \in \mathbb{T}_h$ is a cell containing the point A. As reference value of $p(A)$, we use the result obtained on a very fine uniform mesh.

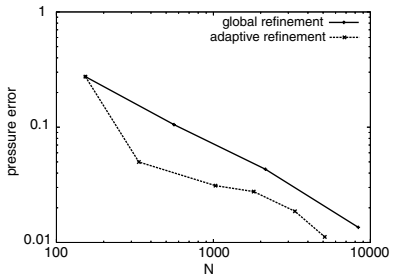

Fig. 8. Reduction of the pressure value error.

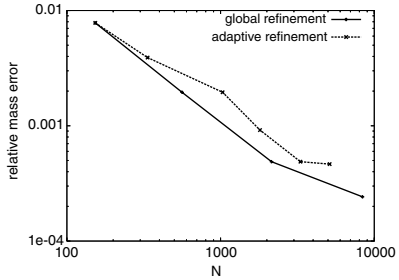

Fig. 9. Relative error of mass conservation.

In Figures 8 and 9 the resulting pressure error and the relative error in mass conservation is displayed as a function of the number of mesh cells. Figure 10 shows a sequence of adapted meshes. As expected two effects can be seen. There is local refinement around the point of interest and since the position of the fluid-structure interface is a decisive factor for the pressure field, local refinement also occurs along the interface.

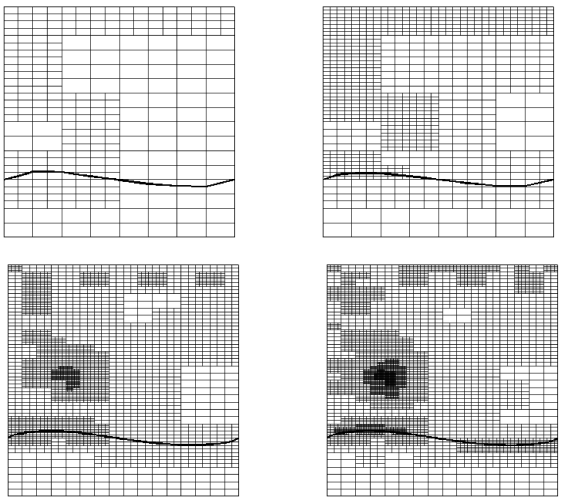

Fig. 10. Locally adapted meshes with $N = 335, 1031, 3309, 5123$ cells.

It may seem surprising that in Figure 9 there is no reduction of the mass error in the last iteration. This is due to the approach we are using here. After each step of mesh adaption a new primal solution is calculated, starting with the initial state of no deformation. The sensitivity analysis though does not take the initial state into account. Mesh adaption takes place around the

final state of the interface, it does not reflect its initial state. An easy way of alleviating the mass error problem is to explicitly move a certain amount of local refinements with the interface from one time step to the next. Doing that though in this example would have made it unclear if the local refinement at the final interface position was due to the sensitivity analysis or the explicit movement of interface-bound refinement.

6 Numerical Test 2: FSI Benchmark FLUSTRUK-A

The second example is the FSI benchmark FLUSTRUK-A described in [15]. A thin elastic bar immersed in an incompressible fluid develops self-induced time-periodic oscillations of different amplitude depending on the material properties assumed. This benchmark has been defined to validate and compare the different computational approaches and software implementations for solving FSI problems. In order to have a fair comparison of our Eulerian-based method with the traditional Eulerian-Lagrangian approach, we have also implemented an ALE method for this benchmark problem.

The configuration of this benchmark shown in Figure 11 is based on the successful CFD benchmark 'flow around a cylinder', [30].

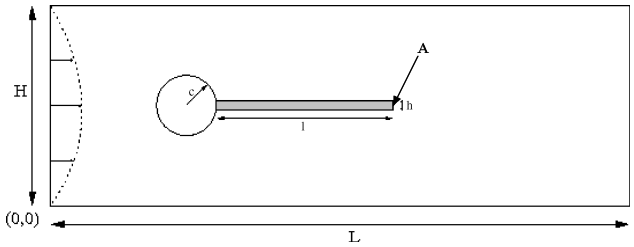

Fig. 11. Configuration of the FSI benchmark 'FLUSTRUK-A'.

Configuration: The computational domain has length $L = 2.5$, height $H = 0.41$, and left bottom corner at $(0, 0)$. The center of the circle is positioned at $C = (0.2, 0.2)$ with radius $r = 0.05$. The elastic bar has length $l = 0.35$ and height $h = 0.02$. Its right lower end is positioned at $(0.6, 0.19)$ and its left end is clamped to the circle. Control points are $A(t)$ fixed at the trailing edge of the structure with $A(0) = (0.6, 0.20)$, and $B = (0.15, 0.2)$ fixed at the cylinder (stagnation point).

Boundary and initial conditions: The boundary conditions are as follows: Along the upper and lower boundary the usual 'no-slip' condition is used for

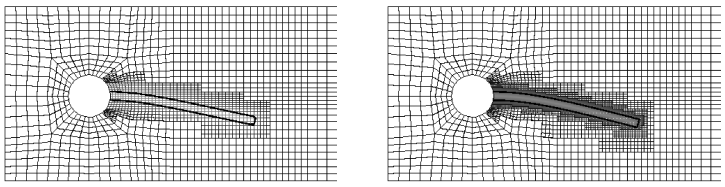

Fig. 12. CSM test: Stationary position of the control point A on heuristically refined meshes with $N = 1952$ and $N = 7604$ cells.

the velocity. At the (left) inlet a constant parabolic inflow profile,

$$v(0, y) = 1.5\,\bar{U}\,\frac{4y(H - y)}{H^2},$$

is prescribed which drives the flow, and at the (right) outlet zero-stress $\sigma \cdot n = 0$ is realized by using the 'do-nothing' approach in the variational formulation, [13,23]. This implicitly forces the pressure to have zero mean-value at the outlet. The initial condition is zero flow velocity and structure displacement.

Material properties: The fluid is assumed as incompressible and Newtonian, the cylinder as fixed and rigid, and the structure as (compressible) St. Venant-Kirchhoff (STVK) type.

Discretization: The first set of computations is done on globally refined meshes for validating the proposed method and its software implementation. Then, for the same configuration adaptive meshes are used where the refinement criteria are either purely heuristic, i.e., based on the cell distance from the interface, or are based on a simplified stationary version of the DWR approach (at every tenth time step) as already used before for the cavity example. In all cases a uniform time-step size of $0.005\,s$ is used. The curved cylinder boundary is approximated to second order by polygonal mesh boundaries as can be seen in Figure 12.

The following four different test cases are considered:

- *Computational fluid dynamics test (CFD Test):* The structure is made very stiff, to the effect that we can compare the computed drag and lift coefficients with those obtained for a pure CFD test (with rigid structure).
- *Computational structure mechanics test (CSM Test):* The fluid is set to be initially in rest around the bar. The deformation of the bar under a vertical gravitational force is compared to the deformation of the same bar in a pure CSM test.
- *FSI tests:* Three configurations are treated corresponding to different inflow velocities and material stiffness parameters, and the Eulerian approach is compared to the standard ALE method.

– *FSI with large deflections:* The fluid is set to be initially in rest around the bar. The gravitational force on the bar is very large, causing a large deformation of the bar and eventually it reaching and running up against the channel wall. This case is difficult for the ALE method but can easily be handled by the Eulerian approach.

6.1 CFD Test

Here, the structure is set to be very stiff, to the effect that we can compare derived drag and lift values with those obtained with a pure CFD approach. The forces are calculated based on the closed path S around the whole structure, cylinder and bar,

$$J(u,p) := \int_S \sigma_f \cdot n \, do. \tag{27}$$

The CFD test has been done with the parameters listed in Table 1.

Table 1. Parameters for the CFD test.

Parameters	CFD test
$\rho_f[10^3 kg\, m^{-3}]$	1
$\nu_f[10^{-3} m^2 s^{-1}]$	1
ν_s	0.4
$\rho_s[10^6 kg\, m^{-3}]$	1
$\mu_s[10^{12} kg\, m^{-1} s^{-2}]$	1
$U[m\, s^{-1}]$	1

For the chosen parameters there is a steady state solution. The reference values for the drag and lift forces are calculated using a pure CFD approach on globally refined meshes (see also [15]). The results are shown in Table 2. Using the Eulerian FSI approach, we calculate the same forces again. As a method of mesh adaption we use a heuristic approach as described above.

Table 2. CFD test: Results of CFD computation on uniform meshes (left), and by the Eulerian FSI approach on heuristically adapted meshes (right).

N	dof	drag	lift
1278	3834	145.75	10.042
4892	14676	133.91	10.239
19128	57384	136.00	10.373
75632	226896	136.54	10.366
300768	902304	136.67	10.369
∞	∞	136.70	10.530

N	dof	drag	lift
1300	9100	122.66	12.68
2334	16338	126.13	11.71
9204	64428	131.77	10.53
36680	256760	134.47	10.45
∞	∞	136.70	10.530

Table 3. Parameters for the CSM test.

parameter	CSM test
$\rho_f[10^3 kg\,m^{-3}]$	1
$\nu_f[10^{-3} m^2 s^{-1}]$	1
ν_s	0.4
$\rho_s[10^3 kg\,m^{-3}]$	1
$\mu_s[10^6 kg\,m^{-1} s^{-2}]$	0.5
$\bar{U}[m\,s^{-1}]$	0
$g[m\,s^{-2}]$	2

Table 4. CSM test: Displacement of the control point A for three levels of heuristic mesh adaption.

N	dof	$u_x(A)$ $[10^{-3}m]$	$u_y(A)$ $[10^{-3}m]$
1952	13664	-5.57	-59.3
3672	25704	-6.53	-63.4
7604	53228	-6.74	-64.6
∞	∞	-7.187	-66.10

6.2 CSM Test

Here, the inflow velocity is set to zero and the fluid is initially at rest. A vertical gravitational force is applied, which causes the bar to slowly sink in the fluid filled volume. Due to the viscous effect of the fluid the bar will eventually come to rest. The value of final displacement can be compared to the results calculated with a pure CSM approach in a Lagrangian framework. The quantity of interest is the displacement of the point A at the middle of the trailing tip. The corresponding reference values are taken from [15]. The CSM test has been done with the parameters listed in Table 3. Using the Eulerian FSI approach, we calculate the displacements with mesh adaption by the heuristic approach described above. The final stationary positions and the heuristically adapted meshes can be seen in Figure 12.

Next, we apply the DWR method as described above to the CSM test case. In the dual problem, we use the Jacobi matrix of the model as presented in Section 4. In the first example the DWR method was always applied to the final stationary state. The results were used for mesh adaption. The generated mesh was then used with the initially unperturbed problem to determine a new final stationary state. In contrast to that approach, we now apply the DWR method at periodic intervals without restarting. To control the resulting mesh adaption at each interval we try to keep the number of nodes N below a certain threshold N_t. This is achieved by reducing refinement and/or increasing coarsening at each interval. As an example we calculate the point-value of the component sum of $u(A)$ at the control point A. The

position x_A is determined from $x_A - u(x_A) = A(0) = (0.6, 0.2)^T$. As a error control functional, we use a regularized delta function at x_A applied to $(e_1 + e_2)^T u$,

$$J(u) = |K_A|^{-1} \int_{K_A} (e_1 + e_2)^T u(x)\, dx\ ,$$

where K_A is the cell in the Mesh $\mathbb{T}_h$ containing the point A.

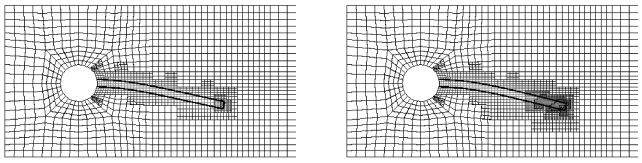

Fig. 13. CSM Test: Stationary position of the bar computed on locally refined meshes (DWR method) with $N = 2016$ and $N = 4368$ cells.

Table 5. CSM Test: Displacements of the control point A for three levels of locally refined meshes (DWR method).

N_t	N	dof	$u_x(A)$ $[10^{-3}m]$	$u_y(A)$ $[10^{-3}m]$
2000	2016	14112	-5.73	-59.8
3000	2614	18298	-6.54	-63.2
4500	4368	30576	-6.88	-64.6
	∞	∞	-7.187	-66.10

6.3 FSI Tests

Three test cases, FSI-2, FSI-3, and FSI-3*, are treated with different inflow velocities and material stiffness values as stated in Table 6. The parameters are chosen such that a visible transient behavior of the bar can be seen. To ensure a 'fair' comparison of results, we calculate the comparison values using the ALE method. Using the Eulerian FSI approach, we calculate the displacements on three mesh levels, where the heuristic approach as described above is used for mesh refinement.

We begin with the FSI-2 and FSI-3 test cases. Some snapshots of the results of these simulations are shown in Figures 14 and 16. The time-dependent behavior of the displacements for the tests are shown in Figures 15 and 17.

The FSI-3* test case is used to illustrate some special features of the Eulerian solution approach. Figure 18 illustrates the treatment of corners in the structure by the IP set approach compared to the LS approach. In the LS method the interface is identified by all points for which $\phi = 0$, while in the

Table 6. Parameter settings for the FSI test cases.

parameter	FSI-2	FSI-2*	FSI-3	FSI-3*
structure model	STVK	STVK	STVK	INH
$\rho_f[10^3 kg\, m^{-3}]$	1	1	1	1
$\nu_f[10^{-3} m^2 s^{-1}]$	1	1	1	1
ν_s	0.4	0.4	0.4	0.5
$\rho_s[10^3 kg\, m^{-3}]$	10	20	1	1
$\mu_s[10^6 kg\, m^{-1} s^{-2}]$	0.5	0.5	2	2
$\bar{U}[m\, s^{-1}]$	1	0	2	2

IP set method the interface is identified by all points which are on one of the

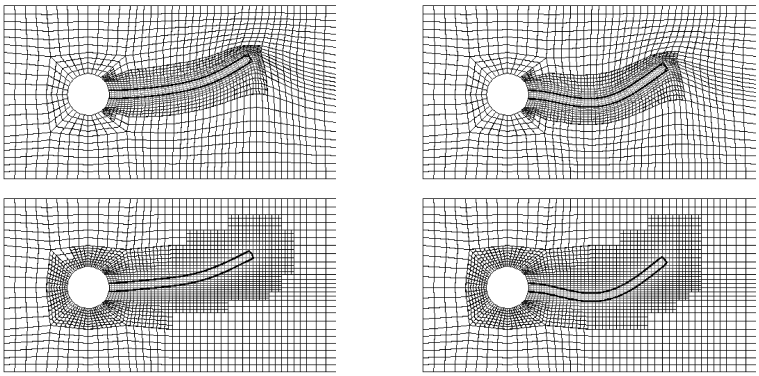

Fig. 14. FSI-2: Snapshots of results obtained by the ALE (top two) and by the Eulerian (bottom two) approaches.

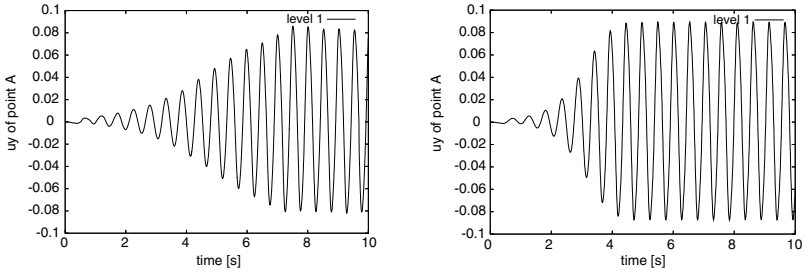

Fig. 15. FSI-2: Vertical displacement of the control point A, obtained by the Eulerian approach (left, $N = 2082$ cells) with maximum amplitude $2.226 \cdot 10^{-2}$ and frequency $1.92\, s^{-1}$, and by the ALE approach (right, $N = 2784$ cells) with maximum amplitude $2.68 \cdot 10^{-2}$ and frequency $1.953\, s^{-1}$.

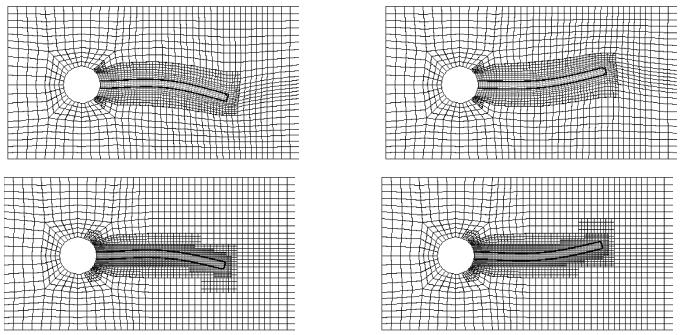

Fig. 16. FSI-3 Test: Some snapshots of results obtained by the ALE (top two) and the Eulerian (bottom two) approaches.

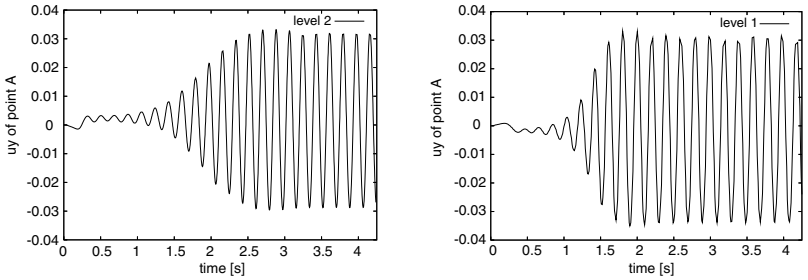

Fig. 17. FSI-3 Test: Vertical Displacement of the control point A, obtained by the Eulerian approach (left, $N = 3876$ cells) with maximum amplitude $6.01 \cdot 10^{-2}$ and frequency $5.48\, s^{-1}$, and by the ALE approach (right, $N = 2082$ cells) with maximum amplitude $6.37 \cdot 10^{-2}$ and frequency $5.04\, s^{-1}$.

respective isoline segments belonging to the edges of the bar. The differences are visible in the cells that contain the corners.

Since in the Eulerian approach the structure deformations are not in a Lagrangian framework, it is not immediately clear, due to the coupling with the fluid, how well the mass of the structure is conserved in an Eulerian approach, especially in the course of an instationary simulation comprising hundreds of time steps. In Figure 19, we display the bar's relative mass error as a function of time. Except for certain initial jitters, the relative error is less than 1%.

Finally, Figure 20 illustrates the time dynamics of the structure and the adapted meshes over the time interval $[0, T]$. More detailed properties of this dynamics is shown in Figure 20. For both approaches, we obtain a periodic

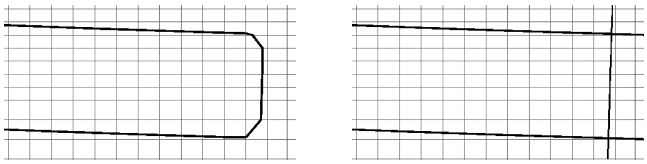

Fig. 18. FSI-3*: Treatment of corners by the LS method (left) and by the IP set method (right).

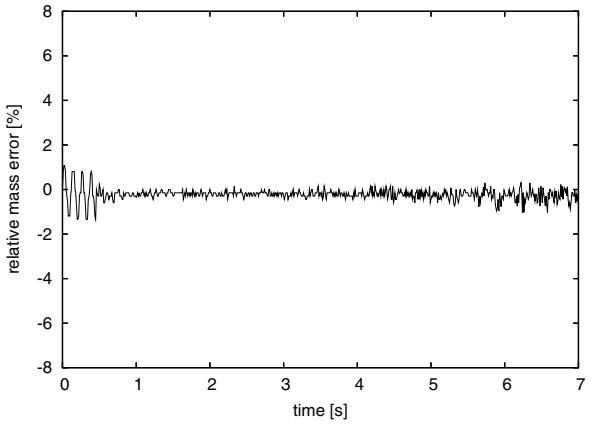

Fig. 19. FSI-3*: Relative mass error of the bar.

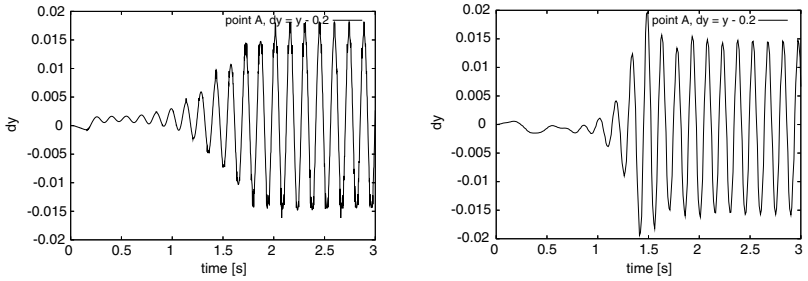

Fig. 20. FSI-3*: Vertical displacement of the control point A, obtained by the Eulerian approach (left) with maximum amplitude $1.6 \cdot 10^{-2}$ and frequency $6.86\, s^{-1}$, and by the ALE approach (right) with maximum amplitude $1.51 \cdot 10^{-2}$ and frequency $6.70\, s^{-1}$.

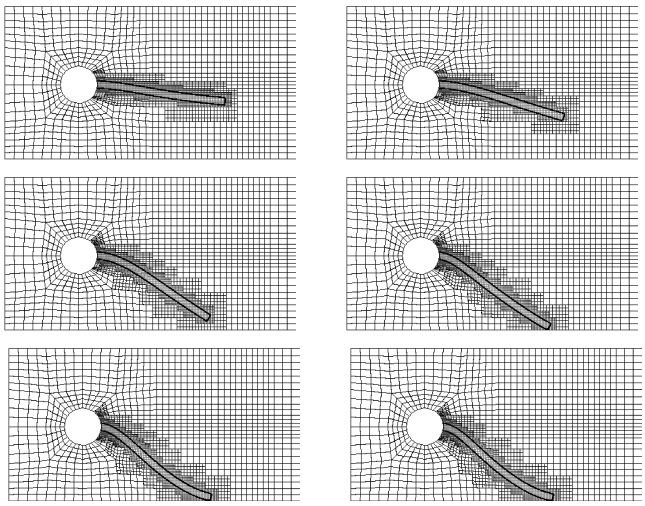

Fig. 21. A sequence of snap-shots of the bar's large deformation under gravitational loading obtained by the Eulerian approach.

oscillation. For the Eulerian approach we obtain an amplitude of 1.6e-2 with an oscillation frequency of $6.86s^{-1}$. In comparison to that, based on the ALE approach, we obtain an amplitude of 1.51e-2 with an oscillation frequency of $6.70s^{-1}$.

6.4 FSI Test with Large Deformations

In the test case FSI-2* (see Table 6) the fluid is initially in rest and the bar is subjected to a vertical force. This causes the bar to bend downward until it touches the bottom wall. A sequence of snapshots of the transition to steady state obtained by the Eulerian approach for this problem is shown in Figure 21. The position of the trailing tip A is show in Figure 22.

7 Summary and Future Development

In this paper we presented a fully Eulerian variational formulation for 'fluid-structure interaction' (FSI) problems. This approach uses the 'initial position' set (IP set) method for interface capturing, which is similar to the 'level set' (LS) method, but preserves sharp corners of the structure. The harmonic continuation of the structure velocity avoids the need of reinitialization of the IP set. This approach allows us to treat FSI problems with free bodies and large deformations. This is the main advantage of this method compared to interface tracking methods such as the arbitrary Lagrangian-Eulerian (ALE)

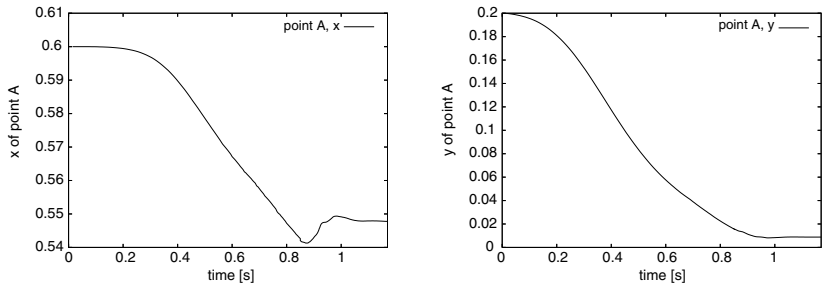

Fig. 22. FSI-2*: Position of the control point A during the deformation of the bar.

method. At several examples the Eulerian approach turns out to yield results which are in good agreement with those obtained by the ALE approach. In order to have a 'fair' comparison both methods have been implemented using the same numerical components and software library GASCOIGNE [33]. The method based on the Eulerian approach is inherently more expensive than the ALE method, by about a factor of two, but it allows to treat also large deformations and topology changes.

The full variational formulation of the FSI problem provides the basis for the application of the 'dual weighted residual' (DWR) method for 'goal-oriented' a posteriori error estimation and mesh adaptation. In this method inherent sensitivities of the FSI problem are utilized by solving linear 'dual' problems, similar as in the Euler-Lagrange approach to solving optimal control problems. The feasibility of the DWR method for FSI problems has, in a first step, been demonstrated for the computation of steady state solutions.

In the next step, we will employ the DWR method also for nonstationary FSI problems, particularly for the simultaneous adaptation of spatial mesh and time step size. Another goal is the development of the Eulerian approach for three-dimensional FSI problems and to explore its potential for FSI problems with large deformations and topology changes. Finally, we intend to extend the variational Eulerian approach and the DWR method to the optimal control of FSI systems.

8 Acknowledgement

This work has been supported by the Deutsche Forschungs Gemeinschaft (DFG, Research Unit 493). This support is gratefully acknowledged.

References

1. W. Bangerth and R. Rannacher, *Adaptive Finite Element Methods for Differential Equations*, Birkhäuser, 2003.

2. R. Becker and M. Braack, A finite element pressure gradient stabilization for the Stokes equations based on local projections, *Calcolo* 38, 173–199 (2001).
3. R. Becker and M. Braack, A two-level stabilization scheme for the Navier-Stokes equations, *Proc. ENUMATH-03*, pp. 123–130, Springer, 2003.
4. R. Becker and R. Rannacher, Weighted a-posteriori error estimates in FE methods, Lecture ENUMATH-95, Paris, Sept. 18–22, 1995, in: *Proc. ENUMATH-97*, (H.G. Bock, et al., eds), pp. 621–637, World Scientific Publ., Singapore, 1998.
5. R. Becker and R. Rannacher, An optimal control approach to error estimation and mesh adaption in finite element methods, *Acta Numerica 2000* (A. Iserles, ed.), pp. 1–101, Cambridge University Press, 2001.
6. R. Becker and R. Rannacher, A feed-back approach to error control in finite element methods: basic analysis and examples, *East-West J. Numer. Math.* 4, 237–264 (1996).
7. M. O. Bristeau, R. Glowinski, and J. Periaux, Numerical methods for the Navier-Stokes equations, *Comput. Phys. Rep.* 6, 73–187 (1987).
8. G. Carey and J. Oden, *Finite Elements, Computational Aspects*, volume III. Prentice-Hall, 1984.
9. Y. C. Chang, T. Y. Hou, B. Merriman, and S. Osher, A level set formulation of Eulerian interface capturing methods for incompressible fluid flows, *J. Comp. Phys.* 123, 449–464 (1996).
10. Th. Dunne. *Adaptive Finite Element Simulation of Fluid Structure Interaction Based on an Eulerian Formulation*, Institute of Applied Mathematics, University of Heidelberg, doctoral dissertation, 2006, in preparation.
11. R. Glowinski. Finite element methods for incompressible viscous flow, in *In Handbook of Numerical Analysis Volume IX: Numerical Methods for Fluids (Part 3)* (P.G. Ciarlet and J.L. Lions, eds), North-Holland, Amsterdam, 2003.
12. K. Eriksson, D. Estep, P. Hansbo, and C. Johnson, Introduction to adaptive methods for differential equations. *Acta Numerica 1995* (A. Iserles, ed.), pp. 105–158, Cambridge University Press, 1995.
13. J. Heywood, R. Rannacher, and S. Turek, *Artificial boundaries and flux and pressure conditions for the incompressible Navier-Stokes equations*, Int. J. Numer. Math. Fluids 22, 325–352 (1992).
14. C. W. Hirt and B. D. Nichols, Volume of Fluid (VOF) method for the dynamics of free boundaries. *Journal of Computational Physics* 39, 201–225 (1981).
15. J. Hron and S. Turek, Proposal for numerical benchmarking of fluid-structure interaction between an elastic object and laminar incompressible flow. In H.-J. Bungartz and M. Schäfer, editors, *Fluid-Structure Interaction: Modelling, Simulation, Optimisation.* to appear in Springer's LNCSE-Series.
16. J. Hron and S. Turek, Fluid-structure interaction with applications in biomechanics. In H.-J. Bungartz and M. Schäfer, editors, *Fluid-Structure Interaction: Modelling, Simulation, Optimisation.* to appear in Springer's LNCSE-Series.
17. A. Huerta and W. K. Liu, Viscous flow with large free-surface motion, *Computer Methods in Applied Mechanics and Engineering*, 1988.
18. D. D. Joseph and Y. Y. Renardy, *Fundamentals of two-fluid dynamics. Part I*, Springer, New York, 1993. Math. Theory and Applications.
19. D. D. Joseph and Y. Y. Renardy, *Fundamentals of two-fluid dynamics. Part II*, Springer, New York, 1993.
20. A. Legay, J. Chessa, and T. Belytschko, An Eulerian-Lagrangian method for fluid-structure interaction based on level sets, *Comp. Meth. in Applied Mech. and Engrg.*, accepted, 2004.

21. C. Liu and N. J. Walkington, An Eulerian description of fluids containing visco-elastic particles, *Arch. Rat. Mech. Anal.* 159, 229–252 (2001).
22. S. Osher and J. A. Sethian, Propagation of fronts with curvature based speed: algorithms based on Hamilton-Jacobi formulations, *Journal of Computational Physics* 79, 12 (1988).
23. R. Rannacher, Finite element methods for the incompressible Navier-Stokes equations, in *Fundamental Directions in Mathematical Fluid Mechanics* (G. P. Galdi, J. Heywood, R. Rannacher, eds), pp. 191–293, Birkhäuser, Basel-Boston-Berlin, 2000.
24. R. Rannacher, Incompressible Viscous Flow, in *Encyclopedia of Computational Mechanics* (E. Stein, et al., eds), John Wiley, Chichester, 2004.
25. R. Rannacher and F.-T. Suttmeier Error estimation and adaptive mesh design for FE models in elasto-plasticity, in *Error-Controlled Adaptive FEMs in Solid Mechanics* (E. Stein, ed.), pp. 5–52, John Wiley, Chichster, 2002.
26. J.A. Sethian, *Level set methods and fast marching methods.* Cambridge University Press, 1999.
27. T. E. Tezduyar, M. Behr, and J. Liou, A new strategy for finite element floow computations involving moving boundaries and interfaces-the deforming-spatial-domain/space-time procedures: I. The concept and preliminary tests, *Computer Methods in Applied Mechanics and Engineering*, 1992.
28. T. E. Tezduyar, M. Behr, and J. Liou, A new strategy for finite element floow computations involving moving boundaries and interfaces-the deforming-spatial-domain/space-time procedures: II. Computation of free-surface ows, two-liquid ows and ows with drifting cylinders, *Computer Methods in Applied Mechanics and Engineering*, 1992.
29. S. Turek, *Efficient solvers for incompressible flow problems: an algorithmic and computational approach*, Springer, Heidelberg-Berlin-New York, 1999.
30. S. Turek and M. Schäfer, Benchmark computations of laminar flow around a cylinder. In E.H. Hirschel, editor, 'Flow Simulation with High-Performance Computers II', volume 52 of *Notes on Numerical Fluid Mechanics.* Vieweg, 1996.
31. W. A. Wall, *Fluid-Structure Interaction with Stabilized Finite Elements*, doctoral dissertation, Report No. 31 (1999), Institute of Structural Mechanics, University of Stuttgart.
32. VISUSIMPLE, An open source interactive visualization utility for scientific computing, `http://visusimple.uni-hd.de/` .
33. GASCOIGNE, A C++ numerics library for scientific computing, `http://gascoigne.uni-hd.de/` .